

ENVIRONMENT-AWARE MIMO CHANNEL ESTIMATION IN PILOT-CONSTRAINED UPPER MID-BAND SYSTEMS

Seyed Alireza Javid and Nuria González-Prelcic

University of California San Diego, USA

ABSTRACT

Accurate multiple-input multiple-output (MIMO) channel estimation is critical for next-generation wireless systems, enabling enhanced communication and sensing performance. Traditional model-based channel estimation methods suffer, however, from performance degradation in complex environments with a limited number of pilots, while purely data-driven approaches lack physical interpretability, require extensive data collection, and are usually site-specific. This paper presents a novel physics-informed neural network (PINN) framework that combines model-based channel estimation with a deep network to exploit prior information about the propagation environment and achieve superior performance under pilot-constrained scenarios. The proposed approach employs an enhanced U-Net architecture with cross-attention mechanisms to fuse initial channel estimates with received signal strength (RSS) maps to provide refined channel estimates. Comprehensive evaluation using realistic ray-tracing data from urban environments demonstrates significant performance improvements, achieving over 5 dB gain in normalized mean squared error (NMSE) compared to state-of-the-art methods, with particularly strong performance in pilot-limited scenarios and robustness across different frequencies and environments with only minimal fine-tuning. The proposed framework maintains practical computational complexity, making it viable for massive MIMO systems in upper mid-band frequencies.

Index Terms— Physics-informed neural network, channel estimation, upper mid-band, MIMO.

1. INTRODUCTION

Channel state information (CSI) is exploited by several functional blocks in a MIMO communication system, including precoding and combining, link adaptation, or equalization [1]. High accuracy CSI is especially important when large arrays are exploited, multiple users (MU) are served, the channel is wideband, or the communication signal is also exploited for localization or sensing [2]. In these scenarios, CSI inaccuracies may lead to beam misalignment, multiuser interference, poor equalization, or reduced sensing accuracy.

Traditional model-based channel estimation techniques for large-array MIMO systems—as those expected in the upper mid-band—often rely on pilots. However, as the number of antennas

increases, they require excessive training and incur high computational complexity, which leads to performance degradation under overhead constraints or in complex propagation environments [3]. Prior work has also proposed black-box, fully data-driven approaches [4, 5, 6] that often suffer from limited physical interpretability, demand large-scale data collection, or tend to generalize poorly beyond the specific site where they were trained. Another line of work combines model-based priors with data-driven learning [7]. However, these combined approaches often utilize the black-box structure of neural networks along with simplistic channel models and unrealistic statistical data for training. Consequently, performance often degrades under domain (site) shift, and substantial site-specific data are required for training when the deployment location changes. Finally, the exploitation of diffusion models in the recent channel estimation literature [7, 6] will also introduce a high overhead in the backward process for generating the channels, and cannot be used in real-time communication systems.

This paper presents the first PINN framework for MIMO channel estimation in the upper mid-band under pilot-constrained scenarios. Unlike prior work that uses PINNs for path loss [8], we integrate RSS maps with LS-based channel estimates through a physics-informed U-Net architecture enhanced with transformers and cross-attention to integrate environmental propagation information with coarse channel information. We validate the design using realistic ray-tracing datasets across frequencies and environments, demonstrating strong generalization. We make the data set available to the research community.

2. PHYSICAL AND COMMUNICATION MODELS

2.1. Physical model

Maxwell's equations govern wireless propagation by linking electric and magnetic fields with material properties [9]. After computing the electric field distribution using numerical methods, the total received power at a given location, or RSS, can be determined from the electric field. Specifically, the received power is proportional to the squared magnitude of the electric field integrated over the receiving antenna's effective area. Mathematically, the RSS accounting for all multipath

components (MPCs), can be expressed as [10]

$$\text{RSS}(\mathbf{r}) = \frac{\lambda^2}{8\pi\eta_0} \left| \sum_{\ell=1}^P E_\ell(\mathbf{r}) \right|^2, \quad (1)$$

where P denotes the number of propagation paths, λ is the wavelength, η_0 is the intrinsic impedance of free space, and E_ℓ represents the complex amplitude of the electric field associated with the ℓ -th path at the receiver location \mathbf{r} . Using $E(\mathbf{r}) = \sum_{\ell=1}^P E_\ell(\mathbf{r})$, this relates to the total electric field. This expression captures the coherent superposition of all paths, including their respective amplitudes and phases.

2.2. Communication channel model

We consider a communication system operating in the upper mid-band (7-24 GHz) in an urban environment. The base station (BS) equipped with a uniform rectangular array (URA) of size $N_t = N_t^x \times N_t^y$ is at the top of a building, and the user equipment (UE) on the ground operating at the same frequency is equipped with a URA consisting of $N_r = N_r^x \times N_r^y$ elements. The frequency selective channel for the d -th channel tap consists of P paths, and can be modeled as

$$\mathbf{H}_d = \sum_{\ell=1}^P \alpha_\ell f_p(dT_s - (t_\ell - t_{\text{off}})) \mathbf{a}_r(\theta_\ell^{\text{az}}, \theta_\ell^{\text{el}}) \mathbf{a}_t(\phi_\ell^{\text{az}}, \phi_\ell^{\text{el}}), \quad (2)$$

where T_s is the sampling interval, t_{off} is the clock offset between the transmitter and receiver, $f_p(\cdot)$ is the filtering function that factors in filtering effects in the system, α_ℓ and t_ℓ are the complex gain and the time-of-arrival (ToA) of the ℓ -th path, $\mathbf{a}_r(\theta_\ell^{\text{az}}, \theta_\ell^{\text{el}})$ represents the receiver array response evaluated at the azimuth and elevation angle-of-arrival (AoA), denoted as θ_ℓ^{az} and θ_ℓ^{el} respectively, and $\mathbf{a}_t(\phi_\ell^{\text{az}}, \phi_\ell^{\text{el}})$ is the transmitter array response evaluated at the azimuth and elevation angle-of-departure (AoD), denoted as ϕ_ℓ^{az} and ϕ_ℓ^{el} respectively. The array responses can be written as

$$\mathbf{a}_r(\theta^{\text{az}}, \theta^{\text{el}}) = \mathbf{a}(\theta'', \theta^\perp) = \mathbf{a}(\theta'') \otimes \mathbf{a}(\theta^\perp) \quad (3a)$$

$$\mathbf{a}_t(\phi^{\text{az}}, \phi^{\text{el}}) = \mathbf{a}(\phi'', \phi^\perp) = \mathbf{a}(\phi'') \otimes \mathbf{a}(\phi^\perp) \quad (3b)$$

where $\theta'' = \cos(\theta^{\text{el}}) \sin(\theta^{\text{az}})$, $\theta^\perp = \sin(\theta^{\text{el}})$, $\phi'' = \cos(\phi^{\text{el}}) \sin(\phi^{\text{az}})$, $\phi^\perp = \sin(\phi^{\text{el}})$, and $\mathbf{a}(\cdot)$ is the steering vector where $[\mathbf{a}(\vartheta)]_n = e^{-j\pi(n-1)\vartheta}$ assuming a halfwave-length element spacing.

2.3. Connecting the physical and the channel models

The electromagnetic analysis models propagation by explicitly computing the electric field from environmental properties. In contrast, communication models approximate the channel as a finite set of paths, each with delay, angle, and complex gain, represented in the MIMO channel matrix $\{\mathbf{H}_d\}_{d=1}^D$ over D delay taps. The physically computed field superposition at each receiver location thus defines the per-tap response in the wideband MIMO channel. Given the transmit power P_T , the

RSS can be calculated per tap, or integrated across all taps, using the MIMO channel matrices, as

$$\text{RSS} = P_T \sum_{d=1}^D \mathbb{E} [\|\mathbf{H}_d\|_F^2], \quad (4)$$

or, equivalently, from the summed field strengths at each tap.

3. RSS-AWARE CHANNEL ESTIMATION

This section describes the proposed PINN framework for low overhead channel estimation. It exploits a few pilots to obtain a coarse channel estimate which is later fused with RSS information to create a refined channel estimate.

3.1. Coarse channel estimation

The first step involves evaluating a coarse channel estimation. To simplify our approach and avoid unnecessary complications, we utilize a basic variation of least squares (LS) estimation [11]. However, the proposed PINN framework can operate with other initial channel estimation methods.

The frequency-selective MIMO channel including all taps is modeled as a 3-dimensional complex tensor $\mathbf{H} \in \mathbb{C}^{D \times N_t \times N_t}$ created by the concatenation of D channel matrices as in (2). The received signal can be written as

$$\mathbf{r}[n] = \sum_{d=0}^{D-1} \mathbf{H}_d \mathbf{s}[n-d] + \mathbf{v}[n], \quad (5)$$

where $\mathbf{s}[n] \in \mathbb{C}^{N_t \times 1}$ is the transmitted pilot vector and $\mathbf{n}_d \sim \mathcal{CN}(0, \sigma_n^2 \mathbf{I})$ is the additive white Gaussian noise. We adopt a simple LS estimator in the frequency domain using OFDM pilots. After LS estimation at pilot subcarriers, magnitude and phase are linearly interpolated to recover the full channel, followed by an inverse FFT to obtain the time-domain taps. This method provides a practical baseline with good initial accuracy for refinement by our physics-informed network.

3.2. Physical calculation

We create the RSS map for the cell of interest using numerical methods. A common tool is *Wireless Insite* [12], which accurately models the electromagnetic environment. We assume the BS has a coarse estimate of the UE's position, allowing us to extract approximate power levels and create the RSS map for network input. In practice, RSS maps can also be generated through digital twins that provide real-time virtual representations of the propagation environment [13].

3.3. Neural network design

We design a physics-informed U-Net with transformer modules, as illustrated in Fig. 1. The three-layer encoder-decoder uses ResNet blocks with skip connections to process the $2 \times D$ channel input. In the latent space, features are fused with RSS embeddings via cross-attention, enabling the network to integrate environmental propagation information with channel structure. The process starts with a projection to a common hidden dimension as

$$\mathbf{X}_i = \mathbf{W}_i \mathbf{F}_i + \mathbf{b}_i ; \quad i \in \{\text{RSS, Channel}\}, \quad (6)$$

where $\mathbf{F}_i \in \mathbb{R}^{\text{Batch} \times D_i}$ is the extracted features from RSS and channel, $\mathbf{X}_i \in \mathbb{R}^{\text{Batch} \times D_z}$ is the projected features, $\mathbf{W}_i \in \mathbb{R}^{D_i \times D_z}$ is the projection matrices, and $\mathbf{b}_i \in \mathbb{R}^{D_z \times 1}$ is the bias vector. Here, D_z represents the dimension of the latent space and D_i is the dimension of RSS or channel features. The cross-attention mechanism employs multi-head attention. The process is formulated as softmax $\left(\frac{\mathbf{Q}\mathbf{K}^T}{\sqrt{D_z}} \right) \mathbf{V}$ where $\mathbf{Q} = \mathbf{X}_{\text{Channel}}$, $\mathbf{K} = \mathbf{X}_{\text{RSS}}$, and $\mathbf{V} = \mathbf{X}_{\text{RSS}}$. Setting \mathbf{Q} as channel features, and \mathbf{K} , \mathbf{V} as RSS features, enables the channel estimation to query what environmental information is most relevant for refinement, where the attention weights determine which RSS spatial patterns are most informative for each channel element. This cross-modal attention allows the network to selectively incorporate physics-based environmental knowledge into the channel estimation process rather than treating them as independent modalities. The fused features are refined by a

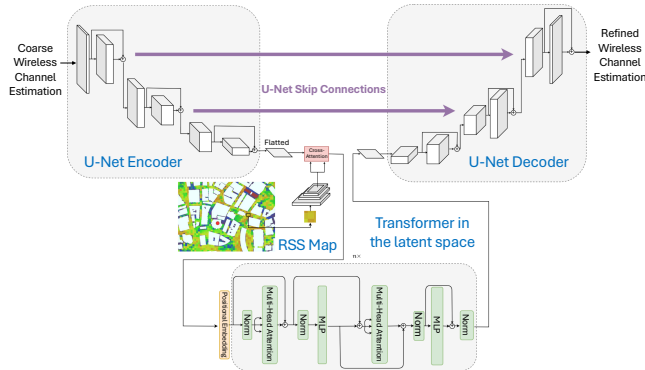


Fig. 1: PINN structure for channel estimation.

transformer with self-attention blocks to capture long-range dependencies and physics-informed relations between RSS patterns and channel characteristics. The decoder mirrors the encoder with transposed convolutions and skip connections to recover the channel dimensions while preserving details. This design combines U-Net's spatial preservation with transformer modeling of channel–environment interactions. Implementation details are given in Section 4.2. Training uses a physics-informed loss that couples Maxwell-based constraints with reconstruction error $\mathcal{L}_{\text{total}} = \mathcal{L}_{\text{NMSE}} + \zeta \mathcal{L}_{\text{phy}}$, where $\mathcal{L}_{\text{NMSE}}$ is the reconstruction loss for the channel estimation defined as

$$\mathcal{L}_{\text{NMSE}} = \mathbb{E} \left(\frac{\|\mathbf{H} - \hat{\mathbf{H}}\|_2^2}{\|\mathbf{H}\|_2^2} \right) \quad (7)$$

in which $\mathbf{H} \in \mathbb{C}^{D \times N_r \times N_t}$ and $\hat{\mathbf{H}} \in \mathbb{C}^{D \times N_r \times N_t}$ are the 3-dimensional complex tensors for accurate and estimated channels respectively. Moreover, \mathcal{L}_{phy} defined as

$$\mathcal{L}_{\text{phy}} = \mathbb{E} \left(\mathbb{E} \left[\frac{\lambda^2}{8\pi\eta_0} \left| \sum_{i=1}^P E_i(\mathbf{r}) \right|^2 \right] - P_T \sum_{d=1}^D \mathbb{E} \left[\left(\|\hat{\mathbf{H}}_d\|_F^2 \right) \right] \right)^2. \quad (8)$$

and ζ weights the physical consistency term to prevent physics violations while maintaining reconstruction accuracy.

Remark. In the pilot-limited regime, the benefit of including the physics-informed term \mathcal{L}_{phy} can be understood through a simple bias–variance argument [14]. Without constraints, a data-driven estimator must search over a high-dimensional hypothesis space, leading to variance scaling as $\text{Var}[f_\theta] \propto d_{\text{eff}}/M$, where f_θ is the neural estimator with parameters θ , d_{eff} is the effective model dimension (less than the model dimension d) and M the number of pilots. By enforcing approximate physical constraints $\mathcal{P}(f_\theta(\mathbf{y})) \approx 0$, with \mathbf{y} the observations (pilots and RSS), the search space is restricted to a lower-dimensional manifold, yielding

$$\text{Var}[f_\theta] \propto d_{\text{eff}}/M, \quad d_{\text{eff}} \ll d, \quad (9)$$

thus reducing estimation variance with only a minor bias if the physical model is imperfect. From an optimization viewpoint, the additional quadratic penalty $\lambda \mathcal{L}_{\text{phy}}$ improves the conditioning of the loss landscape. Writing a gradient step as

$$\theta_{t+1} = \theta_t - \eta (\nabla \mathcal{L}_{\text{data}} + \lambda \nabla \mathcal{L}_{\text{phy}} + \xi_t), \quad (10)$$

where ξ_t denotes stochastic noise, the Hessian gains an extra regularizing term, which lowers the effective condition number and accelerates convergence. Hence, the physics-informed loss improves both generalization and training stability.

4. NUMERICAL EXPERIMENTS

The codes and dataset used to obtain the experimental results presented in this section are provided in [15].

4.1. Dataset

We generated around 10,000 urban channels in Boston using Wireless InSite [12]. The BS was placed on a tall building, and vehicular UEs followed multiple trajectories with different velocities. Each multipath component included amplitude, delay, and angles, and a raised-cosine filter was considered to simulate filtering effects. The RSS maps were also produced to inject physical knowledge into the network. To test adaptability, we constructed datasets at both 8 and 15 GHz, with corresponding bandwidths of 200 and 400 MHz, respectively.

4.2. Network Implementation

Figure 1 shows the encoder, latent domain, and decoder of our network, with layer sizes given in Table 1. We use ResUNet blocks that merge U-Net skip connections with ResNet residuals [16, 17], improving feature propagation and gradient stability for channel estimation. We process RSS inputs with a compact CNN encoder that extracts spatial patterns into a 256-dimensional embedding for channel estimation. It uses stacked 3×3 convolutions with ReLU, 2×2 max-pooling, and a final adaptive pooling layer.

4.3. Numerical Results

Using the hyperparameters in Table 2, we trained with an 80/10/10 train/val/test split. All samples and RSS values were normalized by a fixed constant for consistent NMSE loss scaling. Unless noted otherwise, experiments use $N_t = 24 \times 24$,

Table 1: Physics-Informed U-Net architecture and parameters. \downarrow and \uparrow represent the downsampling and upsampling layers.

Encoder			Latent			Decoder		
#	Type	Output Size	#	Type	Output Size	#	Type	Output Size
Input	Channel	$32 \times 4 \times 576$	1	RSS Encoder	256	Output	Channel	$32 \times 4 \times 576$
1 (\downarrow)	ResUNetBlock	$64 \times 2 \times 288$	2	Cross-Attention	18 432	1 (\uparrow)	ResUNetBlock	$(128 + 128) \times 1 \times 144$
2 (\downarrow)	ResUNetBlock	$128 \times 1 \times 144$	3	Transformer	72×256	2 (\uparrow)	ResUNetBlock	$(64 + 64) \times 2 \times 288$
3 (\downarrow)	ResUNetBlock	$256 \times 1 \times 72$				3 (\uparrow)	ResUNetBlock	$32 \times 4 \times 576$

$N_r = 2 \times 2$, and $D = 16$. We also modeled the channel at an upper-mid band frequency of $f_c = 15$ GHz [18]. We set the number of subcarriers $N = 1024$ and change the subcarrier spacing, and accordingly, the number of pilot signals. We compared the proposed PINN with classical OMP methods[19, 20, 21], a CNN-based estimator [4], and a diffusion model [6]. We focus on performance testing at low-SNR conditions [7] in Figure 2a. We use $N_p = 4$ pilots for PINN and $N_p = 64$ for classical methods. As shown in Figure 2a, PINN outperforms all baselines, achieving ~ 5 dB NMSE gain at SNR = 0, demonstrating robustness in scarce-pilot regimes and the benefit of leveraging environmental information. Moreover, Table 3 highlights the key complexity analysis for the proposed method and [6]. This shows that PINN requires significantly fewer FLOPs and achieves much lower inference latency. The diffusion architecture, however, maintains a low parameter, making it more memory-efficient. Figure 2b shows NMSE vs. pilot count at SNR = 0. CNN and diffusion methods perform well with many pilots, but PINN clearly outperforms in pilot-limited regimes.

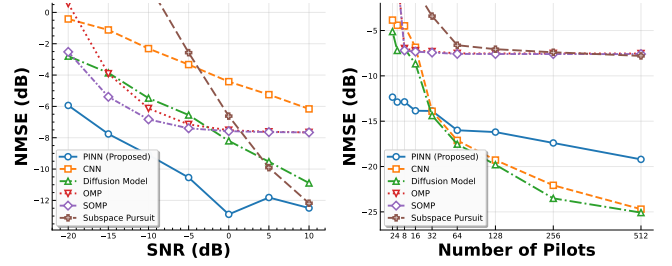
Table 2: Training hyperparameters

Batch	Epochs	LR	Optimizer	ζ
32	500	10^{-3}	Adam	0.01

Table 3: Complexity, latency, and parameters comparison

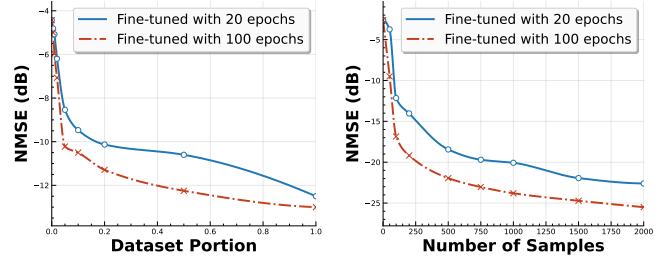
	FLOPs	Latency [ms]	Parameters
(N_t, N_r, D)	(576, 4, 16)	(576, 4, 16)	(576, 4, 16)
PINN	70.85G	11.12	3.5×10^8
DM	130.15G	50.30	5.5×10^4

To evaluate the generalization ability, we tested transfer learning from 15 to 8 GHz (with 400 to 200 MHz bandwidth) using 4 pilots at SNR = 0 dB. As shown in Figure 3, even 10% of the 8 GHz data yields NMSE ≈ -5 dB, while full training reaches ≈ -13 dB. We also transferred from the Boston map to an urban canyon, where the model rapidly adapts: with only 100 samples it achieves NMSE ≈ -9 dB (100 epochs), improving to below -25 dB with 2000 samples. These results confirm that the proposed PINN captures environment-agnostic propagation principles, enabling efficient adaptation across bands and scenarios with limited fine-tuning.



(a) NMSE vs. SNR with $N_p = 4$ (b) NMSE vs. number of pilot signals ($N_p = 64$ for classical methods). nals at SNR = 0 dB.

Fig. 2: NMSE comparison across varying SNRs and pilot counts.



(a) From 15 GHz to 8 GHz in Boston environment (b) From Boston to urban canyon environment

Fig. 3: Transfer learning performance: NMSE vs. dataset for 20 and 100 epoch fine-tuning using $N_p = 4$ and SNR = 0.

5. CONCLUSION

This paper introduced a PINN for accurate wireless channel estimation under pilot-constrained scenarios. By integrating initial simple least-squares estimates with RSS maps derived from Maxwell-based ray tracing, the proposed architecture leverages environmental knowledge through a U-Net backbone enhanced with transformer and cross-attention modules. Our results on realistic 15 GHz urban ray-traced data show that PINN significantly outperforms conventional and learning-based baselines, especially in low-pilot and low-SNR regimes, achieving up to 15 dB NMSE gain over initial LS estimates and over 4 dB gain compared to state-of-the-art models. With low inference latency and strong interpretability, PINN offers a scalable and physically grounded solution for real-time deployment in next-generation MIMO systems.

6. ACKNOWLEDGMENTS

This material is based upon work partially supported by funds from the industry affiliate program at the Center for Wireless Communications (CWC) at UC San Diego.

7. REFERENCES

[1] M. K. Ozdemir and H. Arslan, “Channel estimation for wireless OFDM systems,” *IEEE Communications Surveys & Tutorials*, vol. 9, no. 2, pp. 18–48, 2007.

[2] J. Palacios and N. González-Prelcic, “Separable multidimensional orthogonal matching pursuit and its application to joint localization and communication at mmWave,” in *2023 IEEE Globecom Workshops (GC Wkshps)*. IEEE, 2023, pp. 1421–1426.

[3] J. Palacios, N. González-Prelcic, and C. Rusu, “Multidimensional orthogonal matching pursuit: theory and application to high accuracy joint localization and communication at mmWave,” *arXiv preprint arXiv:2208.11600*, 2022.

[4] M. Sattari, H. Guo, D. Gündüz, A. Panahi, and T. Svensson, “Full-Duplex Millimeter Wave MIMO Channel Estimation: A Neural Network Approach,” *IEEE Transactions on Machine Learning in Communications and Networking*, 2024.

[5] I. Helmy and W. Choi, “Low-Resolution Massive MIMO Channel Estimation with LSTM Attention-Based CBD-Net,” *IEEE Transactions on Mobile Computing*, 2025.

[6] X. Zhou, L. Liang, J. Zhang, P. Jiang, Y. Li, and S. Jin, “Generative diffusion models for high dimensional channel estimation,” *IEEE Transactions on Wireless Communications*, 2025.

[7] Z. Jin, L. You, D. W. K. Ng, X.-G. Xia, and X. Gao, “Near-field channel estimation for XL-MIMO: A deep generative model guided by side information,” *IEEE Transactions on Cognitive Communications and Networking*, 2025.

[8] F. Jiang, T. Li, X. Lv, H. Rui, and D. Jin, “Physics-informed neural networks for path loss estimation by solving electromagnetic integral equations,” *IEEE Transactions on Wireless Communications*, 2024.

[9] N. Ida, *Engineering electromagnetics*. Springer, 2015.

[10] Z. Fu, S. Mukherjee, M. T. Lanagan, P. Mitra, T. Chawla, and R. M. Narayanan, “A Fast Indoor Coverage Prediction Scheme at 60 GHz Based on Image Processing, Geometrical Optics, and Transport Theory,” in *2023 IEEE International Symposium on Antennas and Propagation and USNC-URSI Radio Science Meeting (AP-S/URSI)*. Portland, OR, USA: IEEE, 2023, pp. 1231–1232.

[11] M. Ozdemir and H. Arslan, “Channel estimation for wireless OFDM systems,” *IEEE Communications Surveys and Tutorials*, vol. 9, no. 2, 2007.

[12] Remcom, “Wireless InSite EM Propagation Software,” <https://www.remcom.com/wireless-insite-em-propagation-software>, 2022.

[13] Ericsson Technology Review, “Network Digital Twins: Outlook and Opportunities,” *Ericsson Technology Review*, 2023. [Online]. Available: <https://www.ericsson.com/en/reports-and-papers/ericsson-technology-review/articles/network-digital-twins-outlook-and-opportunities>

[14] C. M. Bishop and N. M. Nasrabadi, *Pattern recognition and machine learning*. Springer, 2006, vol. 4, no. 4.

[15] S. A. Javid and N. González-Prelcic, “Environment-Aware MIMO Channel Estimation in Pilot-Constrained Upper Mid-Band Systems — Code Repository,” https://github.com/ajavid34/PINN_channel-estimation, 2025.

[16] O. Ronneberger, P. Fischer, and T. Brox, “U-net: Convolutional networks for biomedical image segmentation,” in *International Conference on Medical image computing and computer-assisted intervention*. Springer, 2015, pp. 234–241.

[17] K. He, X. Zhang, S. Ren, and J. Sun, “Deep residual learning for image recognition,” in *Proceedings of the IEEE conference on computer vision and pattern recognition*, 2016, pp. 770–778.

[18] S. Kang, M. Mezzavilla, S. Rangan, A. Madanayake, S. B. Venkatakrishnan, G. Hellbourg, M. Ghosh, H. Rahmani, and A. Dhananjay, “Cellular wireless networks in the upper mid-band,” *IEEE Open Journal of the Communications Society*, 2024.

[19] W. Dai and O. Milenkovic, “Subspace pursuit for compressive sensing signal reconstruction,” *IEEE transactions on Information Theory*, vol. 55, no. 5, pp. 2230–2249, 2009.

[20] J. Lee, G.-T. Gil, and Y. H. Lee, “Channel estimation via orthogonal matching pursuit for hybrid MIMO systems in millimeter wave communications,” *IEEE Transactions on Communications*, vol. 64, no. 6, pp. 2370–2386, 2016.

[21] J. A. Tropp and A. C. Gilbert, “Signal recovery from random measurements via orthogonal matching pursuit,” *IEEE Transactions on information theory*, vol. 53, no. 12, pp. 4655–4666, 2007.